ACS Photonics

Article

Cite This: ACS Photonics 2018, 5, 4296−4302

pubs.acs.org/journal/apchd5

Improving the Responsivity of Hybrid Graphene−Conductive Polymer Photodetectors via Nanowire Self-Assembly

Mingxing Li,* Dmytro Nykypanchuk, and Mircea Cotlet*

Center for Functional Nanomaterials, Brookhaven National Laboratory, Upton, New York 11973, United States

Supporting Information

ABSTRACT: By changing the morphology of a poly(3-hexylthiophene) (P3HT) conductive polymer via self-assembly from a planar thin film to a nanowire mesh mesostructure, we demonstrate hybrid graphene−conductive polymer photodetectors with an experimentally observed 600% improved photoresponsivity when compared to their analogous hybrid photodetectors based on graphene and a planar P3HT thin film of similar thickness. At least two reasons stand behind such a dramatic increase in photoresponsivity: (i) the polymer nanowire mesh architecture with unit cell dimensions comparable to the wavelength of light, which produces light scattering and increased light absorption in the polymer compared to the case of a planar polymer thin film of similar thickness, and (ii) the crystallization of P3HT molecules within the nanowires reduces the density of charge trap states, which in turn provides improved charge transport and charge transfer compared to a P3HT thin film.

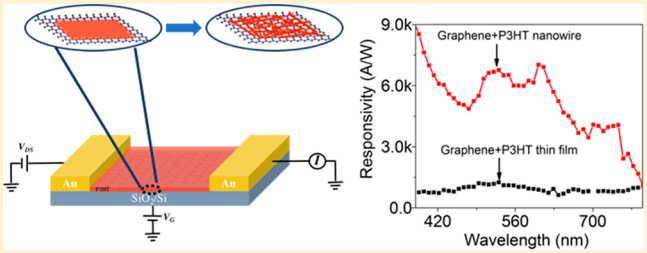

KEYWORDS: *graphene, conductive polymer, hybrid photodetectors, nanophotonics, charge transfer, nanowires*

Atomically thin graphene is an intriguing low-dimensional nanomaterial with unique electronic, mechanical, and optical properties that enable strong light−matter interactions.[1−5] However, graphene's extremely low absorptivity (2.3%), a property inherent to its atomically thin thickness, makes this material's applicability in light-sensing devices somehow shy.[6−10] One alternative way to overcome this problem is to combine graphene with strong light absorbers, for example, with colloidal quantum dot (QD) semiconductors[11−15] or with conductive polymers, materials widely used in organic electronics, including photovoltaics, due to their high absorption cross sections and their ability to be bandgap engineered through chemical synthesis.[16−18] Poly(3-hexylthiophene) (P3HT) is one such example of a conductive polymer that has been intensely investigated for the development of low-cost, highly efficient organic solar cells.[19−21] P3HT has been recently combined with graphene to develop high gain photodetectors,[16] with P3HT−graphene hybrid photodetectors obtained by spin-casting the polymer as a thin film (few tens of nm) on top of graphene. Regioregular (or rr)-P3HT can be self-assembled in nanowires with high aspect ratio and of tens of micrometers long, either by the Whiskers method[22] or by the mixed solvent method.[23] These nanowires already self-assemble in solution, with crystallization being driven by strong $\pi-\pi$ interactions happening perpendicular to the polymer-conjugated backbone and by hydrophobic interactions involving the polymer side chains.[24] The resulting nanowires can therefore be drop- or spin-cast on graphene to form a mesh-like self-assembled mesostructure that can promote light scattering and reabsorption of light by both the polymer and graphene,[25−27] thus further improving the efficiency of a hybrid single-layer graphene (SLG)−P3HT photodetector. Following this rationale, herein we demonstrate successful preparation of P3HT nanowire−graphene hybrid photodetectors by the mixed solvent method and show that such an approach can lead to a 600% improvement in optoelectronic response (photoresponsivity) for the SLG−P3HT nanowire mesh hybrid field effect transistor (FET) when compared to the SLG−P3HT thin film hybrid FET of similar thicknesses. We believe that two key factors contribute to the observed dramatic enhancement: (i) the realization of an optimal nanowire mesh-like mesostructure with unit cell size on the order of the wavelength of light, which produces efficient light scattering and increased light absorption by the polymer and graphene, and (ii) the crystallization of P3HT within the nanowires, which results in decreased charge trapping and, as such, an improved charge transport and charge transfer of the polymer with graphene in comparison to a P3HT thin film.

A cartoon of the SLG−P3HT nanowire hybrid FET is shown in Figure 1a, and an optical image of the pristine graphene FET device is shown in Figure 1b. Confirmation of a SLG was done by atomic force microscopy (AFM), which measured a thickness of 0.52 ± 0.15 nm. This value is slightly larger than the previously reported 0.33 nm[28] and might reflect the presence of (water) molecules trapped between graphene and the SiO_2/Si substrate. Further confirmation of the

Received: April 1, 2018
Published: October 12, 2018

DOI: 10.1021/acsphotonics.8b00420
ACS Photonics 2018, 5, 4296−4302

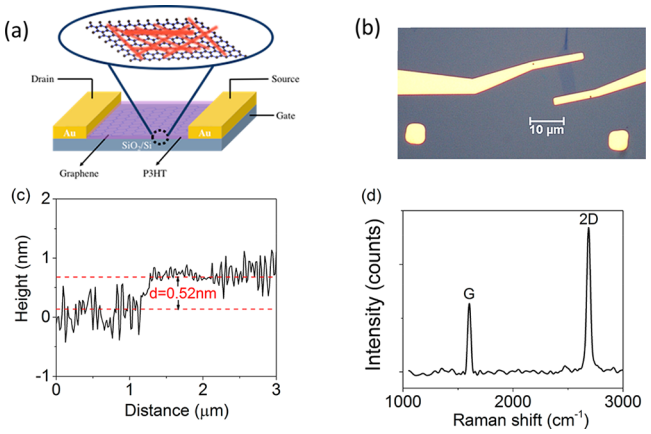

Figure 1. (a) Cartoon of the SLG−P3HT nanowire hybrid FET showing the nanowire mesh (red color) responsible for light scattering and increased light absorption in the polymer, leading to increase hybrid FET photoresponsivity. (b) Optical reflection image of a pristine graphene FET. (c) Graphene thickness estimated by AFM. (d) Raman microspectroscopy of exfoliated graphene on the Si/SiO_2 substrate.

presence of a SLG was by Raman microspectroscopy (Figure 1d), which identified the characteristic G peak at 1603 cm^{-1} and the 2D band at 2690 cm^{-1}, with the two bands featuring an intensity ratio of 2.[28−31]

Using mechanically exfoliated monolayer graphene, we built two types of hybrid FETs, an SLG−P3HT nanowire mesh FET and an SLG−P3HT thin film FET, with the P3HT nanowire mesh and the P3HT thin film of similar thicknesses (~11 nm) as measured by AFM (see Figure S1, Supporting Information, SI). Figure 2a,b and d,e detail the transfer characteristics and output characteristics for the SLG−P3HT thin film FET and the SLG−P3HT nanowire FET, respectively, and they also include similar data for the pristine (graphene-only) FETs from which hybrid FETs were made. For all four FETs the transfer characteristics of drain current vs gate voltage (I_{DS} vs V_G) (Figure 2a,d) were measured for a drain−source voltage V_{DS} = 0.3 V, and the output characteristics of drain current vs drain−source voltage (I_{DS} vs V_{DS}) (Figure 2b,e) were measured for a gate voltage V_G = 30 V and under various light illumination powers.

Pristine FETs show ambipolar transport (Figure 2a,d, black curves), which originates from the zero-bandgap nature of graphene.[32,33] They feature Dirac points (V_D) located at positive values, around 5 and 6 V, respectively, indicating the intrinsic p-type doping of monolayer graphene.[34] Addition of P3HT polymer to an SLG FET decreases the value of V_D due to the hole transfer happening from monolayer graphene to the P3HT polymer (Figure 2a,d, red curves recorded under dark conditions).[18,35] The Dirac point decreases to V_D = −15 V for an SLG−P3HT thin film FET (Figure 2a, red curve recorded under dark conditions), a change of ΔV_D = −20 V, and to V_D = −16 V for an SLG−P3HT nanowire FET (Figure 2d, red curve recorded under dark conditions), a change of ΔV_D = −22 V. The repeatability of our study is further proved by the measurements based on multiple devices (Figure S2, SI). These changes in the Dirac point of graphene with added P3HT suggest that graphene has a lower Fermi level than P3HT and that the energy difference between graphene and P3HT helps holes to be transferred from graphene to P3HT to create a built-in field to equilibrate the Fermi level (see left scheme in Figure 2c, dark conditions). This is consistent with previous reports on the Fermi level for graphene, E_F = −4.6 eV,[34] and on the HOMO and LUMO values for P3HT, E_{HOMO} = −4.9 eV and E_{LUMO} = −3.0 eV, respectively.[36] This type of alignment favors the transfer of photogenerated holes from the p-type P3HT to monolayer graphene (see right scheme in Figure 2c, illumination conditions). Under white light illumination, both hybrid FETs change their Dirac points toward increased positive voltage (Figure 2a,d, blue curves with light vs red curves in the dark), presumably because photogenerated holes are being transferred from P3HT to graphene by the built-in field. Consequently, residual electrons

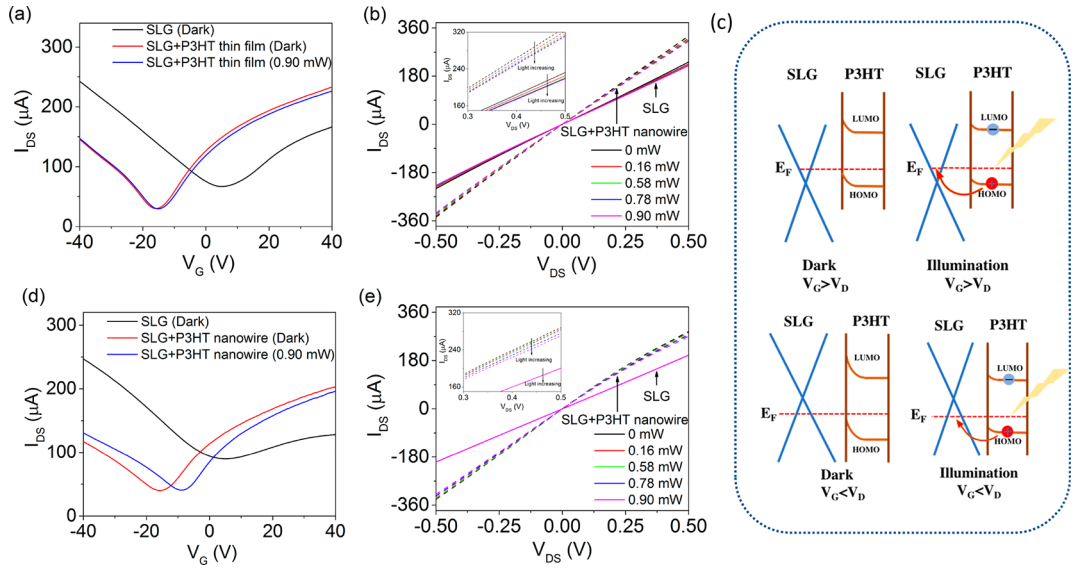

Figure 2. (a and d) Drain current vs gate voltage curves, I_{DS} vs V_G, recorded at V_{DS} = 0.3 V for pristine and hybrid FETs. (b and e) Drain current vs drain voltage curves, I_{DS} vs V_{DS}, recorded at V_G = 30 V for pristine and hybrid FETs. (a) and (b) are for pristine SLG and SLG−P3HT thin film hybrid FETs; (d) and (e) are for pristine SLG and SLG−P3HT nanowire hybrid FETs. (c) Energy band diagram at the SLG−P3HT interface under dark and under illumination conditions.

DOI: 10.1021/acsphotonics.8b00420
ACS Photonics 2018, 5, 4296−4302

left in P3HT generate a top gate voltage, which in turn modifies the carrier concentration and the conductivity of graphene.[12,16,18] When the hybrid FET is operated in the electron conduction region ($V_G > V_D$), the photogenerated holes transferred from P3HT to graphene will compensate the gate-induced free electrons and the residual electrons, thus decreasing the drain current (Figure 2c, upper scheme). Conversely, when the hybrid FET is operated in the hole conduction region ($V_G < V_D$), the photogenerated holes transferred from P3HT to graphene will enhance the hole concentration in graphene, increasing the drain current (Figure 2c, lower scheme).

We next examined the output characteristics of hybrid FETs vs polymer film morphology (thin film vs nanowire mesh) under white light illumination (Figure 2b,e), where we observed small changes in the I_{DS} vs V_{DS} curves with applied illumination power for both hybrid and pristine FET$_S$. For hybrid FETs vs pristine FETs we observed a decrease in the I_{DS} vs V_{DS} characteristic with increased illumination power (Figure 2(b,e) and insets), which we believe is due to a compensation between photogenerated holes transferred from P3HT onto graphene and the gate-induced free and residual electrons. We also observed an increase in photoresponse from pristine to hybrid FETs (Figure 2b,e). Thus, adding a P3HT polymer on top of graphene, whether thin film or nanowire mesh, leads to hole doping and increased charge carrier density in graphene. We also investigated the transport in a P3HT-only FET, thin film, and nanowire mesh and observed by far lower drain currents ($10^5\times$ lower) compared to those observed for hybrid FETs (Figure S3, SI).

To better distinguish the effect of P3HT polymer film morphology on the performance of SLG−P3HT hybrid FETs, we monitored the ratio of the drain current change, $\alpha(\%) = \frac{\Delta I_{DS}}{I_{DS(G)}} = \frac{I_{DS(hybrid)} - I_{DS(G)}}{I_{DS(G)}} \times 100\%$, vs applied V_{DS} vs illumination power, with $I_{DS(hybrid)}$ and $I_{DS(G)}$ being the drain currents measured from hybrid FETs and pristine FETs, respectively. For the two types of hybrid FETs, we monitored $\alpha(\%)$ vs applied V_{DS} for a $V_G = 30$ V and under an illumination power of 0.16 mW (Figure 3a) and $\alpha(\%)$ vs applied

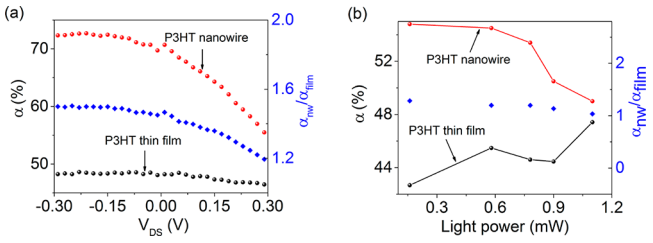

Figure 3. Comparison of drain current change from a P3HT thin film and a P3HT nanowire as a function of (a) bias voltage at $V_G = 30$ V under an illumination power of 0.16 mW and (b) illumination power at $V_{DS} = 0.3$ V and $V_G = 30$ V.

illumination power for $V_{DS} = 0.3$ V and $V_G = 30$ V (Figure 3b). We mention that both P3HT thin film and P3HT nanowires were spin-casted from solutions of 1 mg/mL polymer concentration at a speed of 2000 rpm, a procedure leading to similar thicknesses, as demonstrated by AFM (see SI, Figure S1). As shown in Figure 3a, the P3HT thin film increases the drain current about 48% (Figure 3a, black dots), while the P3HT nanowire mesh increases the drain current about 55−73% (Figure 3a, red dots). This reflects a 1.1−1.5× increase in drain current from a P3HT thin film to a P3HT nanowire mesh (depending on the applied V_{DS}; see Figure 3a, $\alpha_{NW}/\alpha_{film}$, blue dots). Similarly, experiments with varying illumination power (Figure 3b) showed increased drain current for both hybrid FETs when compared to pristine FETs, on average 45% for the thin film FET and 52% for the P3HT nanowires, thus reflecting an average 1.15× larger drain current in the case of P3HT nanowires. We also noticed that the photocurrents from the two hybrid FETs change their sign at similar gate voltage (Figure S4, SI), indicating that our comparison of the performance of the two hybrid FETs is performed in similar responsivity regions. Thus, by changing the morphology of the deposited P3HT polymer one can achieve an improvement in the optoelectronic performance of the hybrid FET.

We observed a dramatic improvement (up to 300%) in the spectral responsivity of the SLG−P3HT nanowire mesh hybrid FET vs the SLG−P3HT thin film hybrid FET and over 3000% vs the pristine (graphene) FETs (Figure 4a and inset). The

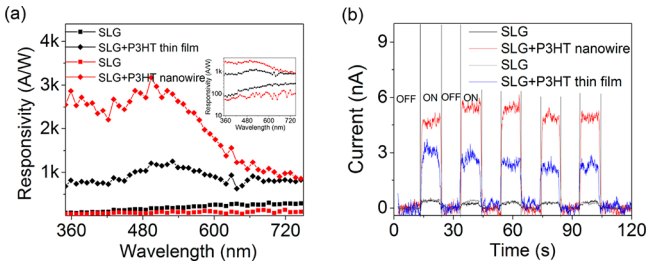

Figure 4. (a) Photoresponsivity spectra from different FET devices under zero bias and $V_G = -40$ V. (b) Transit measurements at zero bias and $V_G = -40$ V by switching the lamp on and off at specific times.

photoresponsivity was estimated as $R = I_{ph}/P_{light}$, with I_{ph} being photocurrent and P_{light} being incident light intensity.[37−40] We also tested the response of the hybrid FETs against on/off illumination and compared the results with those obtained from pristine FETs devices (Figure 4b). We observed similar outperformance of the hybrid SLG−P3HT nanowire FET vs hybrid SLG−P3HT thin film FET (5.3 nA vs 2.3 nA for nanowire vs thin film, e.g., >230% signal increase) and vs pristine FET (5.3 nA vs 0.4 nA, >1300% signal increase), while a clear change was not observed in the response times with on/off illumination with the addition of P3HT ($\tau_{rise(Graphene)} \approx 828 \pm 216$ ms vs $\tau_{rise(Graphene+P3HT\ nanowire)} \approx 296 \pm 38$ ms vs $\tau_{rise(Graphene+P3HT\ thin\ film)} \approx 305 \pm 37$ ms).

The formation of P3HT nanowires is a consequence of strong interchain $\pi-\pi$ stacking driven by the mixed solvent.[24] This strong $\pi-\pi$ stacking can lead to the enhancement of both charge transport and light harvesting, which in turn can increase the drain current in the SLG−P3HT nanowire mesh hybrid FET.[41−45] Two hypotheses can be proposed in order to explain the observed enhancement in the hybrid FET's photoresponse following a change in polymer morphology from thin film to nanowire mesh: (i) *scattering of incident light by the nanowire mesh mesostructure, leading to reabsorption of light by the polymer and graphene*. Nanowires can increase the polymer−light interaction path length and interaction dwell time following multiple scattering events when compared to the case of a thin film.[46] Furthermore, previous reports show

DOI: 10.1021/acsphotonics.8b00420
ACS Photonics 2018, 5, 4296−4302

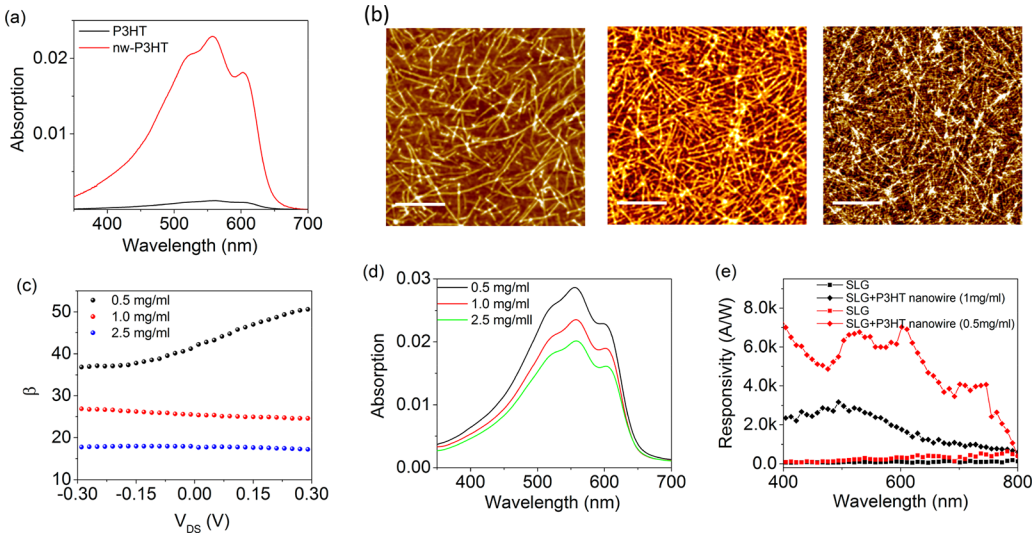

Figure 5. (a) Absorption spectra (normalized to volume unit, v) of a P3HT thin film and P3HT nanowire mesh of similar (11 nm) thickness, each spin-casted from a 1 mg/mL polymer solution. (b) AFM images of P3HT nanowire mesh samples spin-casted from solutions of 0.5 mg/mL (left), 1.0 mg/mL (middle), and 2.5 mg/mL (right) polymer concentration. Scale bar in images is 1 μm. (c) Drain current change, $\beta = \frac{\alpha}{v}$, vs V_{DS}, with drain current change values normalized to the nanowire unit volume, v, for P3HT nanowires mesh spin-casted from solutions of different polymer concentrations. (d) Absorption spectra (normalized to volume unit, v) of P3HT nanowire mesh samples spin-casted from solutions of different polymer concentrations. (e) Photoresponsivity spectra from pristine graphene FETs and hybrid SLG−P3HT nanowire mesh FETs spin-casted from solutions of different polymer concentrations. Spectra were recorded at zero bias and at $V_G = -40$ V.

that P3HT nanowires can increase the out-of-plane and in-plane extinction coefficients ($k_\perp$ and $k_\parallel$) in the transversal- and longitudinal-polarized incidences, enhancing the absorption of P3HT.[47,48] The second hypothesis is (ii) *an enhancement in the electric conductivity of the polymer as a result of self-assembly in nanowires.* The drain current in the hybrid FET depends on carrier density and mobility, and it can be expressed as $I = nq\mu E$, with n being carrier density, q unit charge, μ mobility, and E electric field. Transferred holes from P3HT to graphene will change the carrier density n, thus contributing to the drain current, and this is observed for both types of hybrid FETs (Figure 2b,e). An improvement in crystallization of P3HT reduces the traps in P3HT, which increases the mobility in P3HT to help more holes move to the interface between P3HT and graphene, resulting in more holes transferring to graphene.[49,50] This changes the carrier density and the drain current correspondingly. Below we discuss experimental facts in support of both hypotheses.

Figure 5a shows normalized absorption spectra (to volume unit of polymer sample) for a P3HT thin film and a P3HT nanowire mesh of similar thickness, with the absorption of the P3HT nanowire mesh mesostructure being 20× stronger compared to that of the P3HT thin film. We mention that both samples accounting for Figure 5a were obtained by spin-casting solutions of 1 mg/mL polymer concentration, leading to similar film thickness (Figure S1, SI). From the AFM image in Figure S5, SI, we estimated the number of nanowires per area unit and calculated the amount of polymer per volume unit to find this amount to be 12× smaller compared to a thin film sample of similar area size and film thickness (see the SI for detailed explanation of calculations). These observations strongly suggest that the nanowire mesh mesostructured architecture induces light scattering and reabsorption of light onto the polymer and graphene compared to a plain thin film, and this in turn enhances the drain current in the SLG−P3HT nanowire mesh hybrid FET compared to the thin film based hybrid FET. To further confirm this hypothesis, we fabricated a set of SLG−P3HT nanowire mesh hybrid FETs using solutions of P3HT of various concentrations, 0.5 mg/mL (Figure 5b, left), 1.0 mg/mL (Figure 5b, middle), and 2.5 mg/mL (Figure 5b, right). As such, we achieved different thicknesses and nanowire densities for the mesh mesostructures composing the hybrid FET. From the AFM images in Figure 5b we learned that, by increasing the polymer concentration, we increased the nanowire density toward a continuous film at high concentration (2.5 mg/mL). For the P3HT nanowire mesh, light scattering and light reabsorption should reach a maximum when voids between different nanowires are on the order of the wavelength of light. This seems to be the case of the nanowire mesh formed from the 0.5 mg/mL polymer solution (Figure 5b, left, ∼400 nm voids). Nanowires formed from 1.0 and 2.5 mg/mL P3HT solutions were more crowded, with voids around and below 200 nm, respectively. The absorption spectra of the P3HT nanowire mesh mesostructures of varying polymer concentration (0.5, 1.0, and 2.5 mg/mL) are presented in Figure 5d, and they are normalized to their respective unit volume, e.g., $\gamma = \frac{\mathrm{Abs}}{v}$, with v being a parameter representing the nanowire volume of the unit area. The peak intensity of these absorption spectra decreases with increased nanowire density (increased polymer concentration), an observation that again confirms that light scattering and light reabsorption decrease in samples with increased nanowire density, e.g., with thicker nanowire mesh samples. Further spetroscopic evidence of this claimed effect is provided by the photoluminescence (PL) spectra of the nanowire mesh mesostructures (Figure S6, SI). For these PL spectra, the ratio of the low- and high-energy regions is an indication of the light rescattered and reabsorbed by the film, and this ratio decreases with increased nanowire mesh density, e.g., increased polymer concentration. We followed the implication of polymer morphology on the hybrid FET performance. We compared the effect of scattering and

DOI: 10.1021/acsphotonics.8b00420
ACS Photonics 2018, 5, 4296−4302

reabsorption in the three SLG−P3HT nanowire mesh hybrid FETs by normalizing the ratio of the drain current change, α_{NW}, to the unit volume of the P3HT nanowire mesh, ν, thus obtaining $\beta = \frac{\alpha}{\nu}$. Figure 5c shows the β vs V_{DS} dependency decreasing with increased polymer concentration in the nanowire mesh samples, thus reconfirming the trend observed in the absorption spectra from Figure 5d.

When comparing the photoresistivity data for SLG−P3HT nanowire FETs of similar nanowire mesh thickness, but of different nanowire density, e.g., nanowire meshes formed from polymer solutions of 0.5 and 1 mg/mL (Figure 5e), the graphene nanowire mesh hybrid FET made out of a 0.5 mg/mL polymer solution shows a photoresponsivity of around 6000 A/W, or 2× larger than that made out of a 1 mg/mL polymer solution. As such, we can claim that the experimentally observed photoresponsivity improvement following a change in polymer morphology from thin film to nanowire mesh reaches a value of 600%.

We performed X-ray scattering experiments to investigate the crystallinity of the P3HT thin film and of the P3HT nanowire mesh samples. The X-ray diffraction profiles of P3HT thin films and nanowire mesh made from 1 mg/mL polymer concentration and of similar thickness are shown in Figure 6a. The P3HT thin film exhibits a weak and broad peak

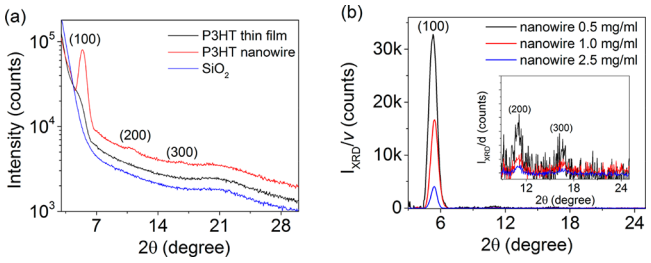

Figure 6. (a) X-ray diffraction profiles of a P3HT thin film and a P3HT nanowire mesh fabricated from a concentration of 1 mg/mL polymer. Offsets are added to the curves for clarity. (b) Normalized X-ray diffraction profiles of P3HT nanowires, $\frac{I_{XRD}}{\nu}$, with I_{XRD} being the intensity of the X-ray diffraction signal and ν the nanowire mesh volume. Data were background subtracted.

corresponding to the (1 0 0) plane at $2\theta \approx 5°$, while the P3HT nanowire shows a stronger and much sharper peak at (1 0 0) plane at $2\theta \approx 5.4°$. For P3HT nanowires, there are two additional peaks corresponding to the (2 0 0) plane at $2\theta \approx 10.9°$ and the (3 0 0) plane at $2\theta \approx 16.7°$. Thus, the X-ray data strongly suggest enhanced packing of the alkyl side chain and enhanced crystallinity of P3HT in the nanowire vs thin film. While the diffraction peaks corresponding to P3HT lamellae are clearly visible, the peak corresponding to $\pi-\pi$ stacking, the (0 2 0) plane, expected at $2\theta \approx 23°$ cannot be discerned. Absence of this peak might be indicative of strong orientation of the crystalline domains with respect to the substrate surface. The scans presented in Figure 6a were performed out of the sample plane, and they will only show crystalline planes oriented parallel to the substrate surface. The difference in crystallinity between P3HT thin films and P3HT nanowires of similar thickness is further demonstrated by grazing-incidence small-angle X-ray scattering (GISAXS) measurements (Figure S7 in the SI). There are clear diffraction patterns for P3HT (1 0 0) in the q_z axis for nanowires, while no such patterns are seen for P3HT thin films. Additionally, only strong diffraction spots are observed along the q_z direction from P3HT nanowires; these results show that crystalline domains are highly oriented in the nanowire mesh samples with lamellae planes parallel to the surface and with the $\pi-\pi$ stacking direction along the surface. Additionally, GISAXS of P3HT thin films and P3HT nanowires deposited on graphene also show similar patterns (Figure S8 in the SI), indicating that graphene does not change the crystallization of P3HT. This crystalline orientation is typically referred to in the literature as edge-on orientation.[49] In contrast, for the thin films, not only is crystallinity almost absent, but also the alignment of crystallite domains is much weaker compared to nanowire meshes. Generally, grain boundaries between disordered chains, residual doping, and other structures or chemical traps can introduce localized trap states in conductive polymers, including P3HT.[51,52] The enhanced crystallization of P3HT observed by X-ray in the case of nanowires can be responsible for the reduced density of trap states. This in turn may lead to enhanced charge mobility in the nanowire vs thin film and, as a result, to improved optoelectronic performance in SLG−P3HT nanowire mesh hybrid FETs.[51,53−55] In Figure 6b we also compared the volume-normalized X-ray diffraction profiles of three P3HT nanowire mesh samples of different polymer concentrations (Figure S9 in the SI), 0.5, 1, and 2.5 mg/mL, to highlight that the intensity of the peak (1 0 0) decreases with increased concentration of the nanowire mesh, thus indicating that the crystallization decreases in the thicker nanowire mesh mesostructures. This is consistent with the phenomenon that fewer nanowires are formed in the thicker nanowire mesh mesostructures, as shown in Figure 5b.

In summary, we demonstrated a simple and straightforward method to dramatically improve the optoelectronic properties of hybrid graphene−conductive polymer FETs. We demonstrated hybrid SLG−P3HT nanowire photodetectors with 600% experimentally observed improvement in spectral photoresponsivity over analogous hybrid devices based on P3HT thin films of similar thickness. We reasoned that (i) improved charge transfer from increased crystallinity and (ii) enhanced light scattering and light reabsorption in the nanowire mesh mesostructure over the thin film are the two main factors accounting for the observed dramatic optoelectronic enhancement.

MATERIALS AND METHODS

Device fabrication, mixed solvent deposition and self-assembly process, electronic and optical measurements, AFM thickness measurements, and GISAXS measurements are detailed in the SI.

ASSOCIATED CONTENT

Supporting Information

The Supporting Information is available free of charge on the ACS Publications website at DOI: 10.1021/acsphotonics.8b00420.

Additional information (PDF)

AUTHOR INFORMATION

Corresponding Authors

*E-mail: mili@bnl.gov.
*E-mail: cotlet@bnl.gov.

ORCID

Mircea Cotlet: 0000-0002-5024-3540

DOI: 10.1021/acsphotonics.8b00420
ACS Photonics 2018, 5, 4296−4302

Notes

The authors declare no competing financial interest.

■ ACKNOWLEDGMENTS

This work was carried out at the Center for Functional Nanomaterials, Brookhaven National Laboratory, which is supported by the U.S. Department of Energy, Office of Basic Energy Sciences, under Contract No. DE-SC0012704.

■ REFERENCES

(1) Novoselov, K. S.; Fal, V.; Colombo, L.; Gellert, P.; Schwab, M.; Kim, K. A roadmap for graphene. *Nature* **2012**, *490* (7419), 192−200.
(2) Bonaccorso, F.; Sun, Z.; Hasan, T.; Ferrari, A. Graphene photonics and optoelectronics. *Nat. Photonics* **2010**, *4* (9), 611−622.
(3) Avouris, P. Graphene: electronic and photonic properties and devices. *Nano Lett.* **2010**, *10* (11), 4285−4294.
(4) Bao, Q.; Loh, K. P. Graphene photonics, plasmonics, and broadband optoelectronic devices. *ACS Nano* **2012**, *6* (5), 3677−3694.
(5) Withers, F.; Bointon, T. H.; Craciun, M. F.; Russo, S. All-graphene photodetectors. *ACS Nano* **2013**, *7* (6), 5052−5057.
(6) Liu, C.-H.; Chang, Y.-C.; Norris, T. B.; Zhong, Z. Graphene photodetectors with ultra-broadband and high responsivity at room temperature. *Nat. Nanotechnol.* **2014**, *9* (4), 273−278.
(7) Xia, F.; Mueller, T.; Lin, Y.-m.; Valdes-Garcia, A.; Avouris, P. Ultrafast graphene photodetector. *Nat. Nanotechnol.* **2009**, *4* (12), 839.
(8) Nair, R. R.; Blake, P.; Grigorenko, A. N.; Novoselov, K. S.; Booth, T. J.; Stauber, T.; Peres, N. M.; Geim, A. K. Fine structure constant defines visual transparency of graphene. *Science* **2008**, *320* (5881), 1308−1308.
(9) Mueller, T.; Xia, F.; Avouris, P. Graphene photodetectors for high-speed optical communications. *Nat. Photonics* **2010**, *4* (5), 297.
(10) Gan, X.; Shiue, R.-J.; Gao, Y.; Meric, I.; Heinz, T. F.; Shepard, K.; Hone, J.; Assefa, S.; Englund, D. Chip-integrated ultrafast graphene photodetector with high responsivity. *Nat. Photonics* **2013**, *7* (11), 883.
(11) Klekachev, A. V.; Cantoro, M.; Van der Veen, M.; Stesmans, A. L.; Heyns, M. M.; De Gendt, S. Electron accumulation in graphene by interaction with optically excited quantum dots. *Phys. E* **2011**, *43* (5), 1046−1049.
(12) Konstantatos, G.; Badioli, M.; Gaudreau, L.; Osmond, J.; Bernechea, M.; De Arquer, F. P. G.; Gatti, F.; Koppens, F. H. Hybrid graphene-quantum dot phototransistors with ultrahigh gain. *Nat. Nanotechnol.* **2012**, *7* (6), 363−368.
(13) Sun, Z.; Liu, Z.; Li, J.; Tai, G. a.; Lau, S. P.; Yan, F. Infrared photodetectors based on CVD-grown graphene and PbS quantum dots with ultrahigh responsivity. *Adv. Mater.* **2012**, *24* (43), 5878−5883.
(14) Zhang, D.; Gan, L.; Cao, Y.; Wang, Q.; Qi, L.; Guo, X. Understanding Charge Transfer at PbS-Decorated Graphene Surfaces toward a Tunable Photosensor. *Adv. Mater.* **2012**, *24* (20), 2715−2720.
(15) Huang, Y.; Zhu, R.; Kang, N.; Du, J.; Xu, H. Photoelectrical response of hybrid graphene-PbS quantum dot devices. *Appl. Phys. Lett.* **2013**, *103* (14), 143119.
(16) Huisman, E. H.; Shulga, A. G.; Zomer, P. J.; Tombros, N.; Bartesaghi, D.; Bisri, S. Z.; Loi, M. A.; Koster, L. J. A.; van Wees, B. J. High gain hybrid graphene−organic semiconductor phototransistors. *ACS Appl. Mater. Interfaces* **2015**, *7* (21), 11083−11088.
(17) Chang, P.-H.; Tsai, Y.-C.; Shen, S.-W.; Liu, S.-Y.; Huang, K.-Y.; Li, C.-S.; Chang, H.-P.; Wu, C.-I. Highly Sensitive Graphene−Semiconducting Polymer Hybrid Photodetectors with Millisecond Response Time. *ACS Photonics* **2017**, *4* (9), 2335−2344.
(18) Tan, W. C.; Shih, W. H.; Chen, Y. F. A Highly Sensitive Graphene-Organic Hybrid Photodetector with a Piezoelectric Substrate. *Adv. Funct. Mater.* **2014**, *24* (43), 6818−6825.
(19) Scharber, M. C.; Mühlbacher, D.; Koppe, M.; Denk, P.; Waldauf, C.; Heeger, A. J.; Brabec, C. J. Design rules for donors in bulk-heterojunction solar cells−Towards 10% energy-conversion efficiency. *Adv. Mater.* **2006**, *18* (6), 789−794.
(20) Li, M.; Wang, H.; He, L.; Zang, H.; Xu, H.; Hu, B. Optically tunable spin-exchange energy at donor: acceptor interfaces in organic solar cells. *Appl. Phys. Lett.* **2014**, *105* (2), 023302.
(21) Liang, Y.; Xu, Z.; Xia, J.; Tsai, S. T.; Wu, Y.; Li, G.; Ray, C.; Yu, L., For the bright future—bulk heterojunction polymer solar cells with power conversion efficiency of 7.4%. *Adv. Mater.* **2010**, *22* (20), E135.
(22) Ihn, K. J.; Moulton, J.; Smith, P. Whiskers of poly(3-alkylthiophene)s. *J. Polym. Sci., Part B: Polym. Phys.* **1993**, *31* (6), 735−742.
(23) Berson, S.; De Bettignies, R.; Bailly, S.; Guillerez, S. Poly(3-hexylthiophene) Fibers for Photovoltaic Applications. *Adv. Funct. Mater.* **2007**, *17* (8), 1377−1384.
(24) Kiriy, N.; Jähne, E.; Adler, H.-J.; Schneider, M.; Kiriy, A.; Gorodyska, G.; Minko, S.; Jehnichen, D.; Simon, P.; Fokin, A. A. One-dimensional aggregation of regioregular polyalkylthiophenes. *Nano Lett.* **2003**, *3* (6), 707−712.
(25) Kim, J. S.; Lee, J. H.; Park, J. H.; Shim, C.; Sim, M.; Cho, K. High-efficiency organic solar cells based on preformed poly (3-hexylthiophene) nanowires. *Adv. Funct. Mater.* **2011**, *21* (3), 480−486.
(26) Wang, X.; Luo, H.; Sun, Y.; Zhang, M.; Li, X.; Yu, G.; Liu, Y.; Li, Y.; Wang, H. Narrow band gap D−A copolymer of indacenodithiophene and diketopyrrolopyrrole with deep HOMO level: Synthesis and application in field-effect transistors and polymer solar cells. *J. Polym. Sci., Part A: Polym. Chem.* **2012**, *50* (2), 371−377.
(27) McCulloch, I.; Ashraf, R. S.; Biniek, L.; Bronstein, H.; Combe, C.; Donaghey, J. E.; James, D. I.; Nielsen, C. B.; Schroeder, B. C.; Zhang, W. Design of semiconducting indacenodithiophene polymers for high performance transistors and solar cells. *Acc. Chem. Res.* **2012**, *45* (5), 714−722.
(28) Gupta, A.; Chen, G.; Joshi, P.; Tadigadapa, S.; Eklund, P. Raman scattering from high-frequency phonons in supported n-graphene layer films. *Nano Lett.* **2006**, *6* (12), 2667−2673.
(29) Ferrari, A. C.; Meyer, J.; Scardaci, V.; Casiraghi, C.; Lazzeri, M.; Mauri, F.; Piscanec, S.; Jiang, D.; Novoselov, K.; Roth, S. Raman spectrum of graphene and graphene layers. *Phys. Rev. Lett.* **2006**, *97* (18), 187401.
(30) Calizo, I.; Balandin, A.; Bao, W.; Miao, F.; Lau, C. Temperature dependence of the Raman spectra of graphene and graphene multilayers. *Nano Lett.* **2007**, *7* (9), 2645−2649.
(31) Akhavan, O.; Ghaderi, E. Differentiation of human neural stem cells into neural networks on graphene nanogrids. *J. Mater. Chem. B* **2013**, *1* (45), 6291−6301.
(32) Novoselov, K. S.; Geim, A. K.; Morozov, S. V.; Jiang, D.; Zhang, Y.; Dubonos, S. V.; Grigorieva, I. V.; Firsov, A. A. Electric field effect in atomically thin carbon films. *Science* **2004**, *306* (5696), 666−669.
(33) Geim, A. K.; Novoselov, K. S. The rise of graphene. In *Nanoscience And Technology: A Collection of Reviews from Nature Journals*; World Scientific, 2010; pp 11−19.
(34) Yu, Y.-J.; Zhao, Y.; Ryu, S.; Brus, L. E.; Kim, K. S.; Kim, P. Tuning the graphene work function by electric field effect. *Nano Lett.* **2009**, *9* (10), 3430−3434.
(35) Sung, Y.-M.; Hsu, F.-C.; Wang, D.-Y.; Wang, I.-S.; Chen, C.-C.; Liao, H.-C.; Su, W.-F.; Chen, Y.-F. Enhanced charge extraction in inverted hybrid photovoltaic cells assisted by graphene nanoflakes. *J. Mater. Chem.* **2011**, *21* (43), 17462−17467.
(36) Shrotriya, V.; Li, G.; Yao, Y.; Chu, C.-W.; Yang, Y. Transition metal oxides as the buffer layer for polymer photovoltaic cells. *Appl. Phys. Lett.* **2006**, *88* (7), 073508.
(37) Gan, X.; Lv, R.; Zhang, T.; Zhang, F.; Terrones, M.; Kang, F. Transferrable polymeric carbon nitride/nitrogen-doped graphene films for solid state optoelectronics. *Carbon* **2018**, *138*, 69−75.
(38) Wang, Q.-M.; Yang, Z.-Y. Graphene photodetector with polydiacetylenes acting as both transfer-supporting and light-

DOI: 10.1021/acsphotonics.8b00420
ACS Photonics 2018, 5, 4296−4302

absorbing layers: Flexible, broadband, ultrahigh photoresponsivity and detectivity. *Carbon* **2018**, *138*, 90−97.
(39) De Fazio, D.; Goykhman, I.; Yoon, D.; Bruna, M.; Eiden, A.; Milana, S.; Sassi, U.; Barbone, M.; Dumcenco, D.; Marinov, K.; Kis, A.; Ferrari, A. C. High Responsivity, Large-Area Graphene/MoS2 Flexible Photodetectors. *ACS Nano* **2016**, *10*, 8252−8262.
(40) Mehew, J. D.; Unal, S.; Torres Alonso, E.; Jones, G. F.; Fadhil Ramadhan, S.; Craciun, M. F.; Russo, S. Fast and Highly Sensitive Ionic-Polymer-Gated WS2 -Graphene Photodetectors. *Adv. Mater.* **2017**, *29*, 1700222.
(41) Liu, J.; Sheina, E.; Kowalewski, T.; McCullough, R. D. Tuning the Electrical Conductivity and Self-Assembly of Regioregular Polythiophene by Block Copolymerization: Nanowire Morphologies in New Di-and Triblock Copolymers. *Angew. Chem., Int. Ed.* **2002**, *41* (2), 329−332.
(42) Kim, J.-H.; Park, J. H.; Lee, J. H.; Kim, J. S.; Sim, M.; Shim, C.; Cho, K. Bulk heterojunction solar cells based on preformed polythiophene nanowires via solubility-induced crystallization. *J. Mater. Chem.* **2010**, *20* (35), 7398−7405.
(43) Mihailetchi, V. D.; Xie, H.; de Boer, B.; Koster, L. A.; Blom, P. W. Charge transport and photocurrent generation in poly (3-hexylthiophene): methanofullerene bulk-heterojunction solar cells. *Adv. Funct. Mater.* **2006**, *16* (5), 699−708.
(44) Pearson, A. J.; Wang, T.; Lidzey, D. G. The role of dynamic measurements in correlating structure with optoelectronic properties in polymer: fullerene bulk-heterojunction solar cells. *Rep. Prog. Phys.* **2013**, *76* (2), 022501.
(45) Campoy-Quiles, M.; Schmidt, M.; Nassyrov, D.; Peña, O.; Goñi, A.; Alonso, M.; Garriga, M. Real-time studies during coating and post-deposition annealing in organic semiconductors. *Thin Solid Films* **2011**, *519* (9), 2678−2681.
(46) Ko, D.-H.; Tumbleston, J. R.; Zhang, L.; Williams, S.; DeSimone, J. M.; Lopez, R.; Samulski, E. T. Photonic crystal geometry for organic solar cells. *Nano Lett.* **2009**, *9* (7), 2742−2746.
(47) Lin, C.-C.; Lin, Y.-Y.; Li, S.-S.; Yu, C.-C.; Huang, C.-L.; Lee, S.-H.; Du, C.-H.; Lee, J.-J.; Chen, H.-L.; Chen, C.-W. Electric field-assisted self-organization of polymer: fullerene hybrids on the photovoltaic performance. *Energy Environ. Sci.* **2011**, *4* (6), 2134−2139.
(48) Chuang, S.-Y.; Chen, H.-L.; Lee, W.-H.; Huang, Y.-C.; Su, W.-F.; Jen, W.-M.; Chen, C.-W. Regioregularity effects in the chain orientation and optical anisotropy of composite polymer/fullerene films for high-efficiency, large-area organic solar cells. *J. Mater. Chem.* **2009**, *19* (31), 5554−5560.
(49) Sirringhaus, H.; Brown, P.; Friend, R.; Nielsen, M. M.; Bechgaard, K.; Langeveld-Voss, B.; Spiering, A.; Janssen, R. A.; Meijer, E.; Herwig, P. Two-dimensional charge transport in self-organized, high-mobility conjugated polymers. *Nature* **1999**, *401* (6754), 685.
(50) Comoretto, D.; Dellepiane, G.; Marabelli, F.; Cornil, J.; Dos Santos, D.; Bredas, J.; Moses, D. Optical constants of highly stretch-oriented poly (p-phenylene-vinylene): A joint experimental and theoretical study. *Phys. Rev. B: Condens. Matter Mater. Phys.* **2000**, *62* (15), 10173.
(51) Noriega, R.; Rivnay, J.; Vandewal, K.; Koch, F. P.; Stingelin, N.; Smith, P.; Toney, M. F.; Salleo, A. A general relationship between disorder, aggregation and charge transport in conjugated polymers. *Nat. Mater.* **2013**, *12* (11), 1038.
(52) Pingel, P.; Zen, A.; Abellón, R. D.; Grozema, F. C.; Siebbeles, L. D.; Neher, D. Temperature-Resolved Local and Macroscopic Charge Carrier Transport in Thin P3HT Layers. *Adv. Funct. Mater.* **2010**, *20* (14), 2286−2295.
(53) Kleinhenz, N.; Persson, N.; Xue, Z.; Chu, P. H.; Wang, G.; Yuan, Z.; McBride, M. A.; Choi, D.; Grover, M. A.; Reichmanis, E. Ordering of poly (3-hexylthiophene) in solutions and films: Effects of fiber length and grain boundaries on anisotropy and mobility. *Chem. Mater.* **2016**, *28* (11), 3905−3913.
(54) Smith, B. H.; Clark, M. B.; Kuang, H.; Grieco, C.; Larsen, A. V.; Zhu, C.; Wang, C.; Hexemer, A.; Asbury, J. B.; Janik, M. J. Controlling Polymorphism in Poly (3-Hexylthiophene) through Addition of Ferrocene for Enhanced Charge Mobilities in Thin-Film Transistors. *Adv. Funct. Mater.* **2015**, *25* (4), 542−551.
(55) Mazzio, K. A.; Rice, A. H.; Durban, M. M.; Luscombe, C. K. Effect of regioregularity on charge transport and structural and excitonic coherence in poly (3-hexylthiophene) nanowires. *J. Phys. Chem. C* **2015**, *119* (27), 14911−14918.

DOI: 10.1021/acsphotonics.8b00420
ACS Photonics 2018, 5, 4296−4302